INSTRUMENT PROPOSAL FOR TOTAL SCATTERING DIFFRACTOMETER - BRAGI

	Name	Affiliation
Main Proposer	Christopher Garvey	Technical University of Munich (Germany)
Contributors	Artur Glavic Anatoliy Senyshyn Martin Meven Christopher Garvey Helen Playford Germán Salazar Alvarez Sabrina Disch Adam Sapnik Mikhail Feygenson	Paul Scherrer Institut (Switzerland) Technical University of Munich (Germany) Forschungszentrum Jülich (Germany) Technical University of Munich (Germany) ISIS Neutron and Muon Source (UK) Uppsala University (Sweden) University of Duisburg-Essen (Germany) University of Copenhagen (Denmark) European Spallation Source (Sweden)
ESS Contact	Mikhail Feygenson	European Spallation Source (Sweden)

1. EXECUTIVE SUMMARY

BRAGI would be a neutron diffractometer dedicated to total scattering experiments, the first of this kind at the European Spallation Source (ESS). The instrument is optimized to cover a large Q-range by matching measurements from multiple incident wavelengths. The concept utilizes monochromators to extract two distinct wavelengths (0.24 and 0.72 Å) from the fast neutron spectrum, as well as four pulses with wavelength frame multiplication to cover momentum transfers from <0.01 to >50 $Å^{-1}$. In a configuration optimized for studies of materials with different and interesting kinds of positional atomic and magnetic disorder, a constant resolution ΔQ/Q of 1.4% can be achieved over Q = 0.4 - 52 $Å^{-1}$. This perspective will enable a broad range of scientific objectives. BRAGI will nicely complement ESS powder diffractometers DREAM and HEIMDAL, both capable of medium resolution pair-distribution function (PDF) measurements with Q_{MAX} = 25 $Å^{-1}$. However the aim here is an instrument dedicated to PDF measurements and the corresponding science case of a broader range of materials. In terms of the neutron flux, resolution, and Q-coverage, BRAGI will match or outperform its counterparts at ISIS. Considering the rapid growth of the PDF community worldwide, such an instrument is urgently needed to meet the overarching demands of academic and industrial European users for high-quality neutron PDF data.

2. SCIENTIFIC CASE

Neutron diffractometers are still the workhorses of any large-scale neutron scattering facility, with a focus on hard condensed matter. The structural and magnetic phase determination of new materials with neutrons is a prerequisite for fundamental and industrial user cases. At short-pulsed or reactor-based facilities, instruments dedicated to high-resolution or high-flux measurements have become a common practice over the last decade. Both types are dedicated to the study of crystalline materials, where refinement of the Bragg scattering patterns provides the answers, and the diffuse background is not considered. Disorder in the local crystal structure manifests itself in the powder diffraction data as a weak diffuse scattering, which is several orders of magnitude less intense than Bragg diffraction peaks, and it mainly contributes to the background underneath the Bragg peaks. The PDF data is obtained by a Fourier transformation of corrected powder diffraction data. It contains both Bragg and diffuse scattering contributions. Therefore, analysis of the PDF data can reveal any deviation of the local crystal structure from the averaged one obtained with the conventional powder diffraction method. Similar issues, interest in the deviations from the local order, exist in soft-matter; however, the analysis methods aim to understand the (larger) deviations from the local structure are subtly different and often require extensive deuteration strategies. For soft deformable matter such atomic scale structural insight complements the ESS suite of spectrometers and their perspective on diffusive motion on short time-scales.

Emerging novel materials, such as energy storage[1] and defect-engineered thermoelectrics[2], which include a mixture of crystalline and amorphous materials, demand a dedicated total scattering diffractometer. Recent developments in PDF data analysis tools[3, 4] and progress in deuteration[5] have broadened the application of neutron PDF experiments. This increased application of the insight gained from total scattering methods is reflected in the growing number of users, which now includes researchers from soft matter, pharmaceutical, and food science fields. It is illustrated in the number of publications with the keyword “neutron pair-distribution function”, starting from 2003, when the first ToF PDF-dedicated instrument, GEM at ISIS, published the first paper (Fig. 1). The data shows a clear leadership of the US and UK, which is not surprising considering the number of PDF instruments at SNS and ISIS. ISIS hosts three instruments within the disordered materials group, as well as the recently upgraded total scattering diffractometer POLARIS. At the SNS, two instruments (NOMAD

and POWGEN) are true powerhouses for the neutron PDF community. The Multi Physics Instrument at the CSNS has recently entered operation with planned extensions to the low-q capability for applications, for example, to soft matter. A new PDF instrument will be built at SNS-STS in the future.

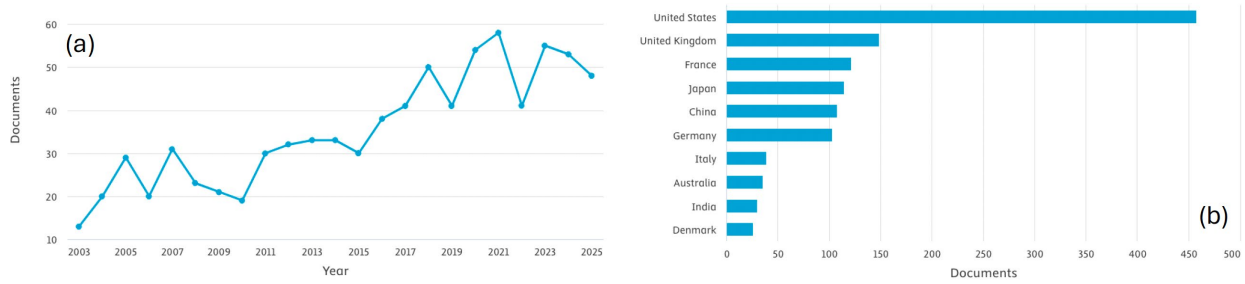

Figure 1 Number of publications for the keyword "neutron pair-distribution function" taken from Scopus from 2003 – 2025: (a) number of publications per year and (b) publications per country.

The scientific case for a dedicated PDF instrument is exceptionally broad, where materials, whether they be crystalline, powdered, textured, gaseous, or liquid, have important structural aspects that can be elucidated from neutron PDF measurements. The major scientific drivers for BRAGI are:

Nanoscale materials:

Exploring how surface functionalization, thermal processing, lithiation, and doping influence the local crystal structure of nanoscale systems is key to tailoring their properties. Such insights are essential for improving their effectiveness in applications including drug delivery, sensing technologies, and battery cathodes.

Liquids and glasses:

In neutron PDF studies of liquids and amorphous materials, isotopic substitution plays a critical role, particularly in revealing hydrogen-bonding networks and solvation effects. A molecular-level understanding of solvent–solute interactions is fundamental for designing greener, environmentally friendly solvent systems and also underlies self-assembly processes. Additional applications include probing solid–liquid interfaces in energy storage systems, studying phase transitions in bulk metallic glasses at elevated temperatures, and examining pressure-induced structural changes in disordered materials.

Quantum materials:

Quantum materials are characterized by macroscopic properties governed by complex quantum mechanical phenomena. Examples include high-temperature superconductors, topological insulators, spin glasses, geometrically frustrated magnets, and systems with unconventional ground states. Neutron PDF techniques enable investigation of how local or metastable disorder influences their ground-state properties.

Confined materials:

Confinement can significantly alter both magnetic behavior and the phase properties of liquids. This is particularly important for hydrogen storage systems and composite magnetic materials. For instance, studying the local structure of nanoconfined water is vital for understanding adsorption behavior, transport in nanoporous media, and phase transitions induced by external fields.

Nucleation and crystallization:

The mechanisms governing nucleation and growth in nanoparticles, liquid crystals, and glassy systems are highly complex, often involving multiple phases and order–disorder transformations. In situ neutron PDF studies of growth dynamics provide valuable insights into how these processes determine the macroscopic properties of both crystalline and amorphous materials. In polymer systems, crystallization and defect formation are equally critical, as they strongly influence material processing and long-term environmental stability.

2.1. Potential new science

High-entropy perovskites

Similar to high-entropy alloys[6], high-entropy perovskites (HEP)[7] are a new class of materials that can benefit from the studies of the local crystal structure. HEP consists of five or more different cations that share the same crystallographic site within the perovskite structure. The unique combination of elements opens up possibilities for novel electronic, magnetic, and optical behaviors, making high-entropy perovskites promising candidates for applications in catalysis, energy storage, and advanced electronics.

The high compositional complexity of HEP leads to increased configurational entropy, providing enhanced structural stability and often enabling single-phase formation despite diverse elemental compositions. In this type of material, a variation of the local crystal structure directly affects the configurational entropy. Even a simple cluster formation reduces the overall entropy due to a decreased number of possible microstates. The neutron PDF measurements will be used to study elemental segregation, precipitation, chemical ordering and spinodal decomposition of HEPs. Single-crystals of HEPs are desirable for gaining more insights into the origin of magnetic interactions, which cannot be obtained from the powder-averaged data. In this case, 3D-PDF measurements will be used (below).

Soft Molecular Materials

While the neutron, x-ray or electron based PDF approach is overcoming the limitations of conventional diffraction in studies of molecular materials[8] within the same conceptual framework in understanding local packing of molecules in soft materials has been limited by extant instrumentation[9]. In particular, the SANS measurement is optimised to determine the shape of molecules/assemblies rather than specific packings of atoms with a structure[10]– such information is complementary. At the atomic scale, soft molecular materials are usefully understood as separate crystalline and amorphous phases, strained materials with nanostructures[11] and 2D materials[12], where this understanding may be productively utilised in processing and the adaptation of emergent materials. To date, the major impact of total scattering measurements is in the characterisation of liquids through the successful user program on the diffractometers at ISIS[13, 14]. More recently, parallel investigations with diffraction[15] and neutron spectroscopy[16] provide important insights for the structure and hydrogen bonding of deep eutectic solvents with applications as green replacements for conventional solvents. For these investigations, there should be an important synergy with VESPA's perspective on the local bonding environment and, more generally, the possibility to make important contributions to the computational description of liquids and dense hydrogen bonded systems.

A more specific example is the use of the PDF to clarify the bonding patterns in non-graphitic carbons and reveal crystallization and disordering mechanisms in pharmaceuticals. The PDF analyses enabled quantification of both crystalline and amorphous phases in pharmaceutical samples, providing essential validation of various formulation processes. An advantage of using neutron PDF for these

types of samples is the possibility of isotope substitution, combined with the absence of radiation damage and the high penetration depth of neutrons. The latter allows for the installation of complex sample environments for the in-situ PDF studies during pharmaceutical formulation.

Local Magnetic Structure of Nanoparticles

Owing to the complexity of new functional materials, novel methods are required to study their magnetic properties on the atomic scale. For example, the interpretation of conventional x-ray and neutron diffraction data of nanoparticles is challenging due to finite-size effects, defects and lack of translational symmetry, so that only limited structural information can be extracted. While the local crystal structure of nanoparticles can be measured by PDF, it is still a challenge to experimentally obtain their local magnetic structure.[17] Numerous studies are devoted to the differences in magnetic structures of nanoparticles and their bulk counterparts. For example, simple 3d-metal oxide materials, the magnetic structure of which is known to be antiferromagnetic in the bulk, show ferromagnetic-like response when their size is reduced down to the nanometer scale. A variety of explanations of such peculiar properties exist in the literature: enhanced magnetic anisotropy of canted spins, defects, increased number of magnetic sub-lattices and so on. Yet, the experimental data on the local magnetic structure needed to distinguish between those effects is still missing. The magnetic PDF (mPDF) formalism aims to probe the local magnetic structure on the atomic scale[18]. Recent advances in mPDF modelling have shown that different orientations of magnetic moments can be distinguished. This is a very promising approach, as it will help us to understand the arrangements of spins throughout the entire volume of magnetic nanoparticles.

Experimental mPDF measurements are challenging and require dedicated instrumentation. Magnetic scattering, often weak, must be separated from strong nuclear and spin-incoherent scattering. The latter is significant in nanoparticles due to the frequent presence of hydrogen in the protective ligand shell surrounding them. There are two general approaches to experimental measurements of the mPDF with neutrons. The first is to model and subtract the nuclear part of the PDF, while the remaining signal is then modelled using the mPDF formalism. The feasibility of this approach has been demonstrated at SNS and ILL beamlines. BRAGI will be well-suited for such measurements. The second approach is to use polarized neutrons and polarization analysis to isolate the magnetic scattering from diffraction data, which can be considered for BRAGI.

Magnetic Liquid Metals

Magnetic Liquid Metals (MLM) are liquid metals that remain in the liquid phase near room temperature[19]. Mercury is the most extensively studied example of MLM. In the past decade, more environmentally friendly MLMs have been synthesized using magnetic nanoparticles. Their ability to transition from liquid to solid phase by adjusting temperature, combined with the capability to morph and change shape under the influence of weak magnetic fields, is a key properties that enable an exciting range of applications. They include magnetic field-responsive metallic ink, ultra-stretchable and deformable electrodes, magnetic and temperature reconfigurable circuit boards, targeted drug delivery, printable body sensors, and more futuristic applications like self-repairing nanorobots. Fundamental interest in MLMs from various research communities is driven by their complex structure, which consists of crystalline nanoparticles dispersed in liquid metals. MLM materials are produced through processes that start from a liquid phase. If the liquid is ferromagnetic or strongly paramagnetic, applying a magnetic field during solidification can have significant and often unexpected effects on the resulting material. Neutron PDF studies will help to investigate these effects and provide the necessary experimental data for theoretical studies. Experimentally, we will use neutron (m)PDF to probe the spin and atomic dynamics in magnetic liquids and to explore novel solidification pathways. This is an uncharted area where the ESS offers unique capabilities: flexible

resolution, intense neutron flux, and advanced computational resources at DMSC. Just as neutron PDF studies of high-entropy alloy solidification using aerodynamic levitation at SNS have impacted the field[65]. Specifically, (m)PDF data will provide insights into the crystal and magnetic structures of nanoparticles, the mechanisms of liquid-to-solid phase transitions, and the role of the nanoparticle–liquid interface. This research not only has the potential to drive scientific innovation but also to generate significant societal benefits through the development of new materials.

Advanced Battery Materials

Neutron scattering has long been recognized as a valuable method for studying Li- and/or Ni-batteries (as well as other types of electrochemical energy storage and conversion, e.g. fuel cells). In contrast to X-rays, neutrons are more sensitive to the light elements such as lithium and oxygen. As a consequence of the ion exchange, ionic transport occurs between the positive and negative electrodes during the operation, causing structural changes in electrode materials. Yet, the exact details of Li-transport and oxygen sublattice distortions remain obscured. The structural changes can range from small distortions of the unit cell to phase transitions. High energy density of battery electrodes are supplemented by the large volumetric changes (up to 400% in Li4.4Si), which can not be accommodated by crystalline materials and require nanosized morphology. Engineering and development of the structural pathway towards new generation intercalation, conversion and alloying-based electrode materials (either for Li, Na, K, Mg etc) is an important development task primary requiring PDF characterizations in different observation mode, e.g. ex and in situ, operando, postmortem etc.

Nanoparticles offer many advantages over existing microsized electrodes especially in the field of high power secondary batteries. For example in nanoparticles, the diffusion length for the Li-ion is several nanometers, limited only to the radial size of a nanoparticle itself. Thus, it takes a shorter time for Li-ion to travel to the particle's surface, where it transfers to the electrolyte. At the same time, the electrode-electrolyte contact area is high due to the large surface area of small nanoparticles. As a result, Li-ion batteries with nanoelectrodes can have higher capacity (energy density), faster charging times (power densities), and longer lifetimes (in terms of capacity and power fade) than state-of-the art electrode materials (Fig. 2).

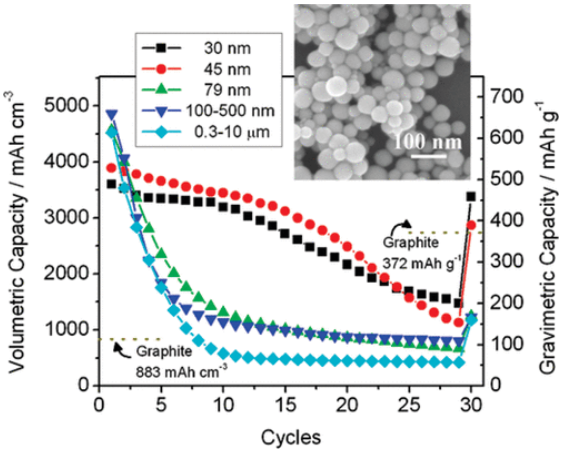

Figure 2 Discharge (Li ion removal) capacities of coin cells with Sn/SnO_x nanoparticles of different diameters as the working electrodes and lithium metal as both the reference and counter electrodes. The dashed line shows the capacity of the graphite-based coin cell (taken from Ref.[20])

A series of pioneering in situ neutron diffraction experiments on Li-ion batteries with the bulk electrodes have been conducted giving rise to understanding and optimization of the underlying processes occurring in real cells under real operating conditions. Development of new generation electrodes with optimized fast transport properties capable to accommodate large volume strains is key for the entire electrochemical energy storage progress. The translational invariance fails in nanosized systems and their properties are driven by the short-range order, surface strains, local dislocations and defects, which requires a dedicated tools and methods. High-quality PDF data is crucial information required by the materials development and optimization, where BRAGI instrument with its wide Q-range, high flux and high-Q resolution fulfills these requirements.

Amorphous Metal–Organic Frameworks

Metal–organic frameworks (MOFs) are a highly functional class of porous materials, with important applications in gas storage and separation, catalysis, and sensing. More recently, amorphous MOFs (aMOFs) have emerged as a class of disordered porous materials in which function is governed by local coordination geometry, linker connectivity, and intermediate-range topology rather than long-range periodicity[21]. For these systems, neutron PDF is uniquely powerful because it provides sensitivity to light elements and isotopes that are difficult to access with X-rays alone, enabling discrimination of metal–ligand correlations, hydrogenous or deuterated linker environments, guest–framework interactions, and disorder in the organic sublattice. This complementarity is especially important for atomistic modelling of aMOFs, where combined X-ray and neutron total scattering can strongly constrain reverse Monte Carlo and related refinements[22]. A key early example was amorphous ZIF-4, for which neutron and X-ray total scattering data were jointly used in reverse Monte Carlo refinement to show that the amorphous phase retains a connected Zn–imidazolate network and is best described as a continuous random network analogous to amorphous silica[23]. With BRAGI, the combination of high flux, large Q-range, and high real-space resolution would make it possible to extend this approach far beyond ZIFs, including direct studies of linker disorder, host–guest structure, isotope-labelled pathways, and in situ amorphization or recrystallization in next-generation aMOFs.

Potential user community

The potential user community for this instrument is exceptionally broad, both in academia and industry sectors. With performance in data collection time, sample size, and sample environments comparable to leading facilities outside the EU, we anticipate attracting a substantial user base, including researchers who currently conduct neutron PDF experiments at SNS and ISIS. Additionally, we expect significant interest from x-ray PDF community from European facilities such as DESY and the ESRF. The primary user communities for BRAGI span fields including nanoscience, battery research, materials science, physical and bioinspired chemistry, green chemistry, pharmaceutical science, hydrogen storage, and quantum materials.

3. AN INITIAL TECHNICAL OVERVIEW OF THE PROPOSED INSTRUMENT, DISCUSSING TECHNICAL FEASIBILITY

The conceptual layout for the BRAGI instrument is shown in Figure 3. There are two extraction pathways: a neutron guide pointed horizontally to the thermal moderator and a downward extraction with a free flight path to a monochromator upstream of the bunker wall that reflects neutrons onto a second monochromator, focusing the beam onto the sample position. The direct beam path through the guide includes a pulse shaping chopper pair as well as a T0 chopper that also acts as a bandwidth selection chopper. The guide is optimized for short wavelength transfer with a relatively low divergence of 1°x1°.

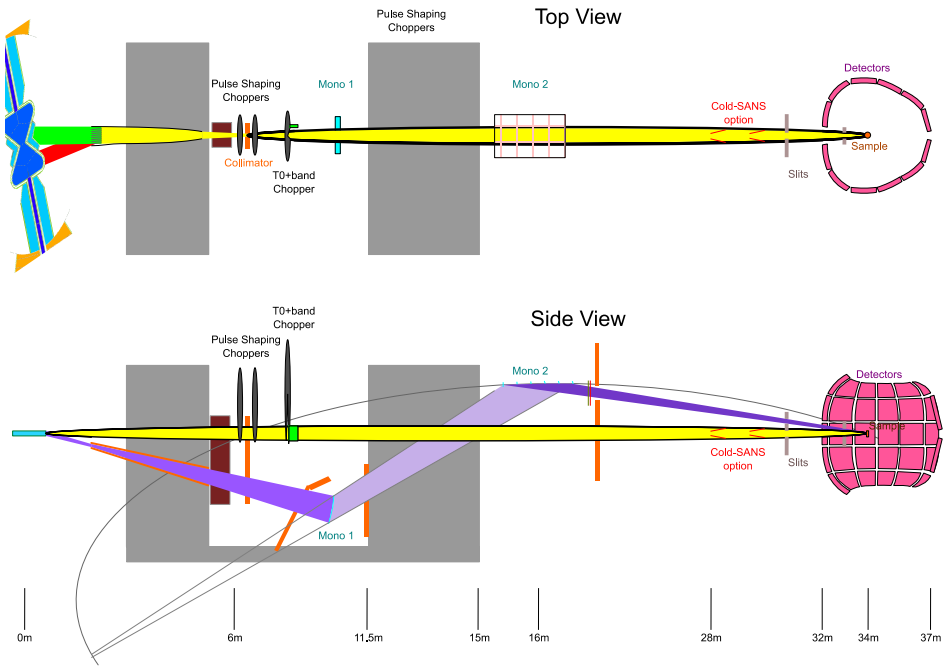

Figure 3: Instrument layout

The bandwidth selection opens only for 4 out of the 5 potential sub-frames generated by the pulse shaping choppers. The remaining closed frame coincides with the beam extracted through the double-monochromator beam path (shown in purple in Figure 3). The two Ge (111) monochromators set to θ=6.36° allow the first and third order reflections (0.723 and 0.241 Å) to reach the sample location, where they are separated enough to be distinguished by flight time. These energies are tuned to a set of filters made of 5.5 mm tungsten and 0.55 mm holmium that suppress higher-order reflections from the monochromators, as shown in Figure 4. The combination of the two filters with the Debye-Waller factor of the monochromators leads to a suppression of all higher orders by at least 5 orders of magnitude. Together with small beam cross-sections at heavy collimation choking points, this will lead to a clean signal at very short wavelengths as well as a larger transported divergence than possible with choppers and conventional neutron guides.

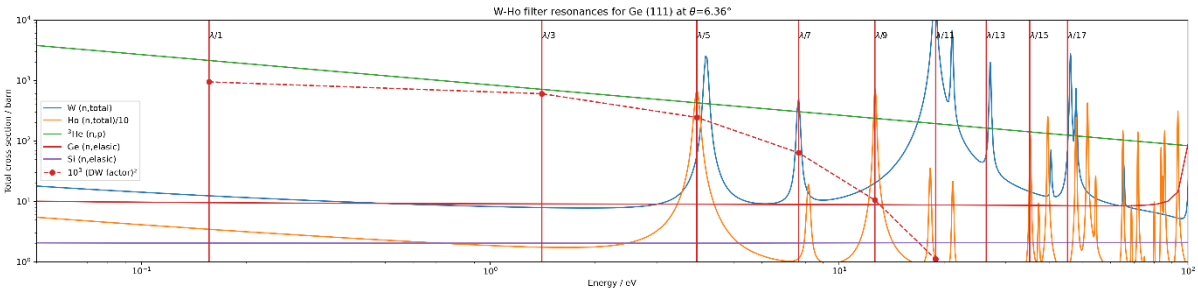

Figure 4: Energy-dependent neutron cross section with the selected orders of the Ge monochromators

A bi-spectral switch in the beam extraction of the direct beam path will combine the thermal and cold moderator spectra of ESS for high performance over the full bandwidth. Figure 5 shows the two distinct wavelengths and WFM bands laid over the ESS moderator spectra. As can be seen, the shortest wavelength that gives access to the highest wavevector transfer makes use of the upturn in the thermal spectrum below 0.5 Å.

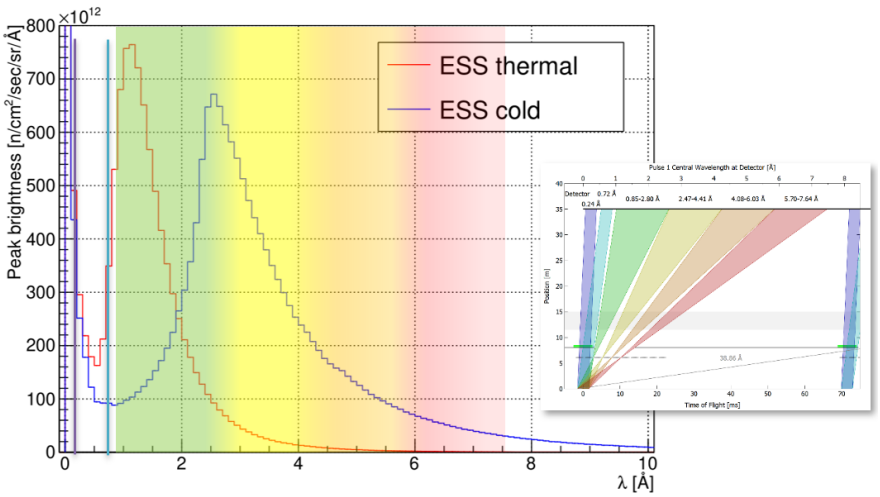

Figure 5: ESS spectrum with individual extracted wavelength by monochromators (purple/blue) and time of flight extraction of thermal and cold spectrum (rainbow); inset shows the corresponding time-distance diagram

The pulse shaping choppers will be placed in a double-blind configuration to allow a fixed Δλ/λ that matches the monochromatic resolution (approx. 1%), leading to around 350mm separation. A heavy collimation block (copper) will be placed between the choppers in the horizontal focus of the parabolic feeder and ballistic guide to reduce fast neutron background. The guide, as well as the monochromators, will be optimized for 1° divergence and 20mm maximum sample size, leading to low background and good performance down to short wavelength, as most of the guide can transport 1 Å neutron with just m=2 coatings.

The secondary flight path consists of a compact sample tank with large solid angle coverage. To minimize detector area and tank volume while limiting the impact on experimental resolution, the detector distance depends on the scattering angle and is optimized using two primary design constraints:

1. An optimized flux-resolution configuration should exist. This configuration has an angular resolution that matches the relative wavelength resolution down to the angle needed for full overlap of the available wavelengths. For 1% wavelength resolution, the combined incident and outgoing angular resolution (including cos(θ) term) should thus match 1% down to the scattering angle where the two distinct wavelengths overlap in Q. (In the case of 3x wavelength, this condition must be fulfilled at 2θ=40°.)
2. The higher angle detector distance should at least match the worst incident divergence for the largest sample. In other words, in such a relaxed resolution case, the detectors should not be the resolution-limiting factor.

The latter gives a minimum detector distance of around 1m, a distance that will not limit any sample environment options either. The resolution matching the required detector distance, depending on sample size, is shown in Figure 6 (left). We define the standard sample size as <=10mm. The detector banks are then positioned at 1m for angles above 100° and curve away from the sample in the forward direction until they reach 3m separation at around 30°. The forward direction is then covered with a flat detector bank perpendicular to the 15° scattered beam direction. The configuration has thus sufficient resolution in the range from 30° to 170°, leading to sufficient overlap between the wavelengths/bands and thus a continuous coverage of Q. If we allow for more relaxed or varying resolution, a larger 2θ range can be used for more flux and lower minimum Q. Figure 6 (right) shows the estimated intensity and Q-dependent relative resolution for some example instrument configurations. For isotropic samples, it could be useful to use asymmetric incident resolution and limit the azimuthal integration area at smaller scattering angles to stay with medium to high

resolution but gain 2x-10x scattering signal above 2θ=90°. The purple lines illustrate the use of a low-Q option based on a focusing device that is employed only for long wavelengths.

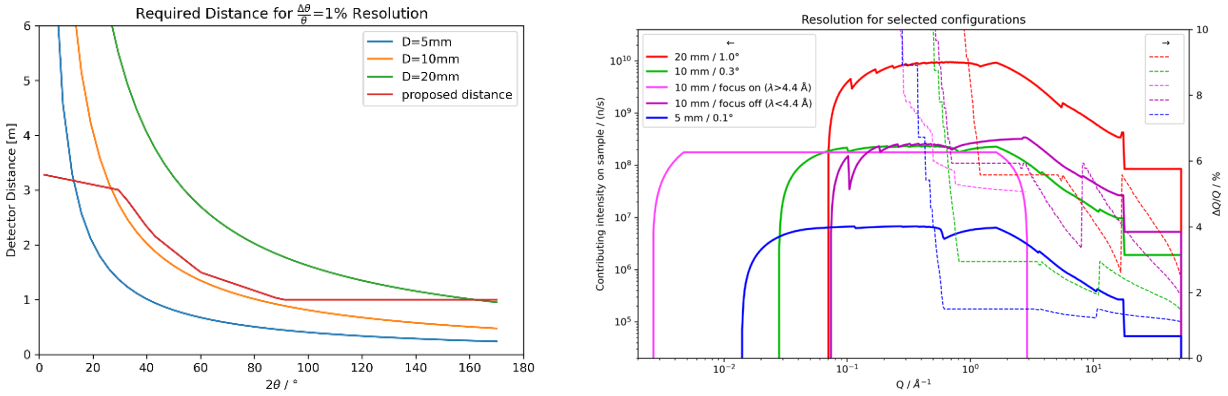

Figure 6: Required detector distance to reach 1% angular resolution with estimated detector placement (left) and calculated total Q-resolution for various sample sizes and incident beam divergences (right)

4. AN EXPLANATION OF HOW THE CONCEPT MAKES USE OF THE ESS LONG-PULSE SOURCE, IF RELEVANT

BRAGI makes use of the ESS's unique capability of bi-spectral extraction to perform diffraction over a large wavelength band effectively (0.85-7.64 Å). In addition, the long pulse and high brilliance is exploited with monochromatic extraction at 0.723 Å and 0.241 Å, which utilizes the upturn in the ESS spectrum for faster neutrons, which is specific to spallation neutron sources. This hybrid time-of-flight approach is only possible at ESS, as continuous sources do not allow separation of the monochromatic wavelengths, and short pulse sources would not have sufficient flux in the individual wavelengths.

5. PLANS OR REQUIREMENTS FOR SAMPLE ENVIRONMENT AND LABORATORY ACCESS

The pool sample-environment equipment for the ESS diffraction instruments DREAM and HEIMDAL will be shared with BRAGI. The broad science case for BRAGI implies a range of sample states, e.g. extremely viscous liquids, that will require specific attention. This broad sample portfolio also necessitates an automatic sample changer equipped with a cryostream, an Orange-type cryostat, a closed-cycle refrigerator with vanadium windows, and an ILL-type vacuum furnace. The electrochemical cell will be required. An aerodynamic levitator is required for containerless (m)PDF studies of solid-to-liquid phase transitions at temperatures above 800 K. Room-temperature magnets will be used for investigations of MLMs and magnetic nanoparticles. Further to the broad scientific scope of BRAGI, a flexible and accessible sample position anticipates additional custom-made sample-environment equipment developed by user communities and tailored specifically to the instrument. Both possible locations of the instrument at the beam ports (N9 or E10) offer easy access to the user laboratories in D buildings.

6. PROPOSED LOCATION OF THE INSTRUMENT AT THE ESS FACILITY, INCLUDING MOTIVATION

BRAGI requires a minimum length of around 35m with only a small width due to the limited divergence and vertical reflection direction of the monochromators. An extension up to around 55m could increase the performance of the 1-5 Å band at the cost of bandwidth and thus the lowest

accessible Q. The instrument could therefore be placed on any of the existing beamline positions. Given that cold neutrons are of lower priority for the instrument concept, an extraction closer to 90° w.r.t. the proton beam would be preferred, and as other beamlines might struggle to fit in those positions, we would propose the use of ports N9 or E10. The highest performance could be reached at E5.

7. GAP ANALYSIS IN TERMS OF BOTH CAPABILITY AND CAPACITY, IN RELATION TO ESS AND THE GLOBAL FACILITY LANDSCAPE.

BRAGI will add the unique capability to reach unprecedented high Q-values of 50 $Å^{-1}$ while covering the full range of neutron diffraction down to 0.02 $Å^{-1}$ (0.003 $Å^{-1}$ if focusing) in a single measurement. This will allow the instrument to reach the best real-space resolution at ESS and expand the diffraction suite with a dedicated instrument for PDF experiments. In the standard ToF band range, BRAGI will be able to perform most single-crystal and powder diffraction PDF experiments and thus expand the capacity in this highly demanded technique. Low-q performance is a significant factor in soft-matter studies. By using a focusing device with short wavelength cut-off together with a pulse-shaping chopper that relaxes wavelength resolution for λ>4.4 Å, the low-Q range can be extended into the SANS-range without limiting the high-Q performance.

8. COMPARISON TO OTHER SIMILAR INSTRUMENTS IN THE WORLD, IF POSSIBLE

The instrument will be one of a kind in Europe. There is only one disordered materials diffractometer at ILL D4, with a typical Q_{max} = 23 A, and lower flux. Other comparable instruments are NOMAD (SNS), GEM, NIMROD (ISIS) and NOVA (J-Parc). While it will be difficult to reach the neutron flux of the NOMAD instrument due to short and intense SNS pulse, the performance of BRAGI will be comparable with GEM in terms of flux and accessible Q-range. The low-Q performance, on the other hand, will surpass these other instruments due to the brightness of the ESS cold moderator.

9. REFERENCES

(1) Liu, F.; Fan, Z. Defect engineering of two-dimensional materials for advanced energy conversion and storage. *Chemical Society Reviews* **2023**, *52* (5), 1723-1772, 10.1039/D2CS00931E. DOI: 10.1039/D2CS00931E.

(2) Wu, C.; Shi, X.-L.; Wang, L.; Lyu, W.; Yuan, P.; Cheng, L.; Chen, Z.-G.; Yao, X. Defect Engineering Advances Thermoelectric Materials. *ACS Nano* **2024**, *18* (46), 31660-31712. DOI: 10.1021/acsnano.4c11732.

(3) Liu, C.-H.; Janke, E. M.; Li, R.; Juhas, P.; Gang, O.; Talapin, D. V.; Billinge, S. J. L. sasPDF: pair distribution function analysis of nanoparticle assemblies from small-angle scattering data. *Journal of Applied Crystallography* **2020**, *53* (3), 699-709. DOI: doi:10.1107/S1600576720004628.

(4) *PDF in the Cloud*. https://pdfitc.org/ (accessed 2026 January 20).

(5) *Deuteration and Macromolecular Crystallisation (DEMAX) platform* https://ess.eu/science-support-systems/demax (accessed 2026 January 20).

(6) Santodonato, L. J.; Zhang, Y.; Feygenson, M.; Parish, C. M.; Gao, M. C.; Weber, R. J. K.; Neuefeind, J. C.; Tang, Z.; Liaw, P. K. Deviation from high-entropy configurations in the atomic distributions of a multi-principal-element alloy. *Nat. Commun.* **2015**, *6* (1), 5964. DOI: 10.1038/ncomms6964.

(7) Banerjee, R.; Chatterjee, S.; Ranjan, M.; Bhattacharya, T.; Mukherjee, S.; Jana, S. S.; Dwivedi, A.; Maiti, T. High-Entropy Perovskites: An Emergent Class of Oxide Thermoelectrics with Ultralow Thermal Conductivity. *ACS Sustainable Chemistry & Engineering* **2020**, *8* (46), 17022-17032. DOI: 10.1021/acssuschemeng.0c03849.

(8) Terban, M. W.; Billinge, S. J. L. Structural Analysis of Molecular Materials Using the Pair Distribution Function. *Chemical Reviews* **2022**, *122* (1), 1208-1272. DOI: 10.1021/acs.chemrev.1c00237.
(9) Garvey, c. j. *ESS Science Symposium on Crystallography for Soft Matter*, 2015.
(10) Hargreaves, R.; Bowron, D. T.; Edler, K. Atomistic Structure of a Micelle in Solution Determined by Wide Q-Range Neutron Diffraction. *Journal of the American Chemical Society* **2011**, *133* (41), 16524-16536. DOI: 10.1021/ja205804k.
(11) Garvey, C. J.; Parker, I. H.; Simon, G. P. On the interpretation of X-ray diffraction powder patterns in terms of the nanostructure of cellulose I fibres. *Macromolecular Chemistry and Physics* **2005**, *206* (15), 1568-1575, Article. DOI: 10.1002/macp.200500008.
(12) Cheng, C.; Jiang, G.; Garvey, C. J.; Wang, Y.; Simon, G. P.; Liu, J. Z.; Li, D. Ion transport in complex layered graphene-based membranes with tuneable interlayer spacing. *Science Advances* **2016**, *2* (2). DOI: 10.1126/sciadv.1501272.
(13) Finney, J. L.; Soper, A. K. Solvent structure and perturbations in solutions of chemical and biological importance. *Chemical Society Reviews* **1994**, *23* (1), 1-10, 10.1039/CS9942300001. DOI: 10.1039/CS9942300001.
(14) Hughes, T.-L.; Falkowska, M.; Leutzsch, M.; Sederman, A. J.; Mantle, M. D.; Headen, T. F.; Youngs, T. G. A.; Bowron, D. T.; Hardacre, C. Bulk and Confined Benzene-Cyclohexane Mixtures Studied by an Integrated Total Neutron Scattering and NMR Method. *Topics in Catalysis* **2021**, *64* (9), 722-734. DOI: 10.1007/s11244-021-01437-w.
(15) Hammond, O. S.; Bowron, D. T.; Edler, K. J. The Effect of Water upon Deep Eutectic Solvent Nanostructure: An Unusual Transition from Ionic Mixture to Aqueous Solution. *Angewandte Chemie International Edition* **2017**, *56* (33), 9782-9785. DOI: https://doi.org/10.1002/anie.201702486 (acccessed 2025/04/17).
(16) Serrano, R. A. F.; Araújo, C. F.; Ribeiro-Claro, P.; Vaz, P. D.; Rudić, S.; Coutinho, J. A. P.; Nolasco, M. M. Decoding disorder: unravelling entropy effects in deep eutectic systems with neutron spectroscopy. *PCCP Phys. Chem. Chem. Phys.* **2025**, *27* (22), 11518-11529, 10.1039/D5CP01144B. DOI: 10.1039/D5CP01144B.
(17) Andersen, H. L.; Frandsen, B. A.; Gunnlaugsson, H. P.; Jorgensen, M. R. V.; Billinge, S. J. L.; Jensen, K. M. O.; Christensen, M. Local and long-range atomic/magnetic structure of non-stoichiometric spinel iron oxide nanocrystallites. *IUCrJ* **2021**, *8* (1), 33-45. DOI: doi:10.1107/S2052252520013585.
(18) Frandsen, B. A.; Fischer, H. E. A New Spin on Material Properties: Local Magnetic Structure in Functional and Quantum Materials. *Chemistry of Materials* **2024**, *36* (19), 9089-9106. DOI: 10.1021/acs.chemmater.4c01535.
(19) Kim, D.; Jeong, J.; Chung, S. K.; Lee, J. B. Magnetic Liquid Metals: A Review. *Advanced Functional Materials* **2024**, *34* (31), 2311153. DOI: https://doi.org/10.1002/adfm.202311153 (acccessed 2026/02/15).
(20) Wang, X.-L.; Feygenson, M.; Aronson, M. C.; Han, W.-Q. Sn/SnOx Core−Shell Nanospheres: Synthesis, Anode Performance in Li Ion Batteries, and Superconductivity. *The Journal of Physical Chemistry C* **2010**, *114* (35), 14697-14703. DOI: 10.1021/jp101852y.
(21) Bennett, T. D.; Cheetham, A. K. Amorphous Metal–Organic Frameworks. *Accounts Chem. Res.* **2014**, *47* (5), 1555-1562. DOI: 10.1021/ar5000314.
(22) Castel, N.; Coudert, F.-X. Atomistic Models of Amorphous Metal–Organic Frameworks. *The Journal of Physical Chemistry C* **2022**, *126* (16), 6905-6914. DOI: 10.1021/acs.jpcc.2c01091.
(23) Bennett, T. D.; Goodwin, A. L.; Dove, M. T.; Keen, D. A.; Tucker, M. G.; Barney, E. R.; Soper, A. K.; Bithell, E. G.; Tan, J.-C.; Cheetham, A. K. Structure and Properties of an Amorphous Metal-Organic Framework. *Physical Review Letters* **2010**, *104* (11), 115503. DOI: 10.1103/PhysRevLett.104.115503.